PROCEEDINGS OF THE
2ND INTERNATIONAL SYMPOSIUM
ON

PROPELLER AND CAVITATION

HANGZHOU CHINA
SEPTEMBER 1–4, 1992

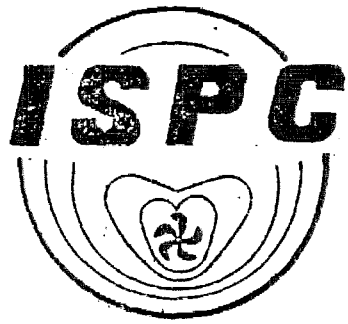

Co-Sponsored by

CHINESE SOCIETY OF NAVAL ARCHITECTURE & MARINE ENGINEERING
(CSNAME, CHINA)
SOCIETY OF NAVAL ARCHITECTS & MARINE ENGINEERS
(SNAME, U.S.A.)
AMERICAN SOCIETY OF MECHANICAL ENGINEERS
(ASME, U.S.A.)

Supported by

CHINA SHIP SCIENTIFIC RESEARCH CENTER
(CSSRC)
SHANGHAI JIAO TONG UNIVERSITY
(SJTU)

CAVITATION SCALING EXPERIMENTS WITH HEADFORMS: BUBBLE DYNAMICS

Yan Kuhn de Chizelle*,
Steven L. Ceccio+,
Christopher E. Brennen*,
Young Shen++

* California Institute of Technology, Pasadena, California, USA
\+ University of Michigan, Ann Arbor, Michigan, USA
++ David Taylor Research Center, Bethesda, Maryland, USA

ABSTRACT

Utilizing some novel instrumentation which allowed detection and location of individual cavitation bubbles in flows around headforms, Ceccio and Brennen (1991 and 1989) recently examined the interaction between individual bubbles and the structure of the boundary layer and flow field in which the bubble is growing and collapsing. They were able to show that individual bubbles are often fissioned by the fluid shear and that this process can significantly effect the acoustic signal produced by the collapse. Furthermore they were able to demonstrate a relationship between the number of cavitation events and the nuclei number distribution measured by holographic methods in the upstream flow. More recently Kumar and Brennen (1991-1992) have closely examined further statistical properties of the acoustical signals from individual cavitation bubbles on two different headforms in order to learn more about the bubble/flow interactions.

However the above experiments were all conducted in the same facility with the same size of headform (5.08cm in diameter) and over a fairly narrow range of flow velocities (around 9m/s). Clearly this raises the issue of how the phenomena identified in those earlier experiments change with changes of speed, scale and facility. The present paper will describe experiments conducted in order to try to answer some of these important questions regarding the scaling of the cavitation phenomena. We present data from experiments conducted in the Large Cavitation Channel of the David Taylor Research Center in Memphis Tennessee, on similar headforms which are 5.08, 25.4 and 50.8cm in diameter for speeds ranging up to 15m/s and for a range of cavitation numbers. In this paper we focus on visual observations of the cavitation patterns and changes in these patterns with speed and headform size.

NOMENCLATURE

C_p	pressure coefficient, $(P_o-P)/(0.5\rho U_o^2)$
D	headform diameter
P	static local pressure
P_o	static free-stream pressure
P_v	water vapor pressure
r	non dimensional bubble radius, R/D
R	bubble radius at the base
Rmax	bubble maximum radius at the base
Re	Reynolds number, U_oD/ν
t	time
U_o	free-stream velocity
X_a	attachment coordinate along axis of revolution
X_c	collapse coordinate along axis of revolution
δ	bubble thickness in the direction normal to the headform surface
ε	bubble sphericity, (δ/R)
ν	kinematic viscosity
ρ	density
σ	cavitation number, $(P_o-P_v)/(0.5\rho U_o^2)$
σ_i	inception cavitation number

1. INTRODUCTION

The purpose of the experiments described herein was to investigate the effects of scale in the cavitation occurring on a simple axisymmetric headform. The focus is on traveling bubble cavitation, and the interaction between the flow and the dynamics and acoustics of individual bubbles. Experiments by Ceccio and Brennen (1991) on 5.08cm diameter axisymmetric headforms had revealed a surprising complexity in the flow around single cavitation bubbles. Among the phenomena observed during those previous experiments were the fact that the bubbles have an approximately hemispherical shape and are separated from the solid surface by a thin film of liquid. This general conformation persists during the growth phase though, especially with the larger bubbles, the thin film appears to become unstable and may begin to shear off the underside of the bubble leaving a cloud of smaller bubbles behind. On the other hand, the collapse phase is quite complex and consists of at least three processes occurring simultaneously, namely collapse, shearing due to the velocity gradient near the surface and the rolling up of the bubbles into vortices as a natural consequence of the first two processes. These processes tend to produce small transverse vortices with vapor/gas filled cores. It was noted that the collapse phase was dependent on the shape of the headform and the details differed between the ITTC headform (Lindgren and Johnsson, 1966) which possessed a laminar separation and the Schiebe body (Schiebe, 1972; Meyer, Billet and Holl, 1989) which did not. The current investigation employed Schiebe headforms which have a minimum pressure coefficient on the surface of $C_{p_{min}}$=-0.78.

Several other features of the flow around individual cavitation bubbles were noted in those earlier experiments and need to be mentioned here. On the ITTC headform, when some of the larger bubbles passed the point of laminar separation they would induce an attached "streak" of cavitation at both the lateral extremes of the bubble as indicated in figure 1. These streaks would stretch out as the bubble proceeded downstream, being anchored at one end to a point on the body surface along the laminar separation line and at the other end to the "wing-tips" of the bubble. The main bubble would collapse, leaving the two streaks it induced to persist longer.

One of the important consequences of these variations in the details of the collapse processes is the effect on the noise produced by a single cavitation event (Ceccio and Brennen, 1991; Kumar and Brennen, 1991-1992). Bubble fission can produce several bubble collapses and therefore several acoustic pulses. Presumably this would also effect the cavitation damage potential of the flow. However it is important to reiterate that these earlier experiments were all conducted with 5.08cm diameter headforms and utilized only a very narrow range of tunnel velocities of 8-9m/s. Consequently there are very real questions as to how the observed

phenomena might scale with both headform size and with tunnel velocity. The experiments described here represent one effort to answer some of these questions.

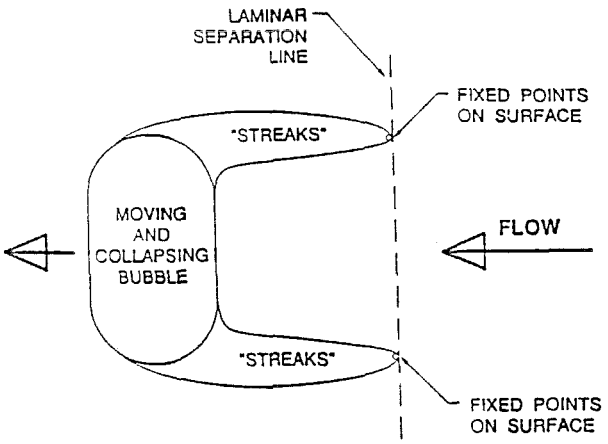

Fig. 1 Schematic diagram indicating the conformation of a cavitating bubble induced separation streaks.

We digress briefly to note that questions on the scaling of cavitation have been asked for many years but particularly in the aftermath of the ITTC comparative tests conducted by Lindgren and Johnsson (1966) who showed how disparate the appearance of cavitation was at different speeds, in different facilities and at different water "qualities". The latter characterization refers to the number of cavitation nuclei present in the water where most of these nuclei usually consist of very small air bubbles in the range 5 to 300μm. As O'Hern et al. (1985, 1988) have shown, these nuclei are similar in size distribution in most deaerated water tunnels and in the ocean. This causes one set of scaling questions since the ratio of body size to the nuclei size will change with the body size. The other set of scaling issues derives from the complex interactions between the bubbles and the flow close to the headform with which the bubbles interact. Since the flow is Reynolds number dependent, scaling effects will also be caused by the changes in both body size and tunnel velocity. As a guide to interpretation of the results of the experiments a panel method was developed to solve the axisymmetric potential flow around the Schiebe headform in the absence of cavitation. Results from these calculations are presented in figure 2, which shows the isobars in the low pressure region near the nose of the headform.

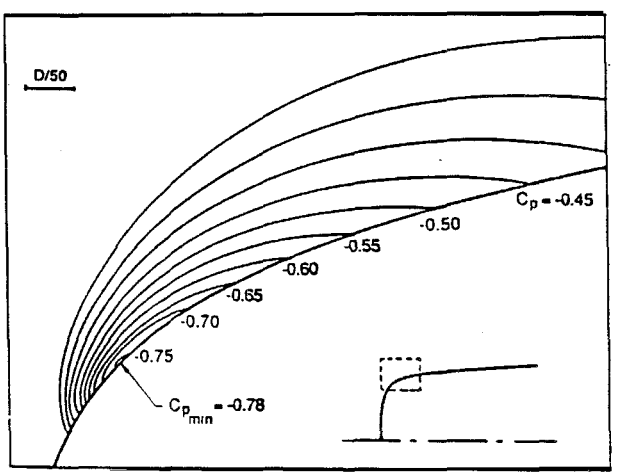

Fig. 2 Pressure distribution around the minimum pressure point in the flow above the Schiebe headform.

2. EXPERIMENTAL SETUP

Large Cavitation Channel

The authors were fortunate to have the opportunity to examine some cavitation scaling effects by conducting experiments in a new facility called the Large Cavitation Channel, which has just been constructed for the David Taylor Research Center (Morgan, 1990). Briefly this facility is a very large water tunnel with a working section which is 3.05m x 3.05m in cross-section. It is capable of tunnel speeds above 15m/s and the pressure control allows operation at sufficiently low pressures in the working section to permit cavitation investigations. Polished lucite windows are located along the side walls of the test section and in the corners at the top and bottom.

Headforms

Three Schiebe headforms of diameter 5.08cm, 25.4cm and 50.8cm were machined out of solid blocks of clear lucite and were mounted in the working section as shown in figure 3. The interiors of the headforms were hollowed out in order to place hydrophones in water within the headform and as close as possible to the cavitation. Lucite was chosen for its good acoustical match with water in addition to its electrically insulating properties. The inside of the headform was filled with water at atmospheric pressure.

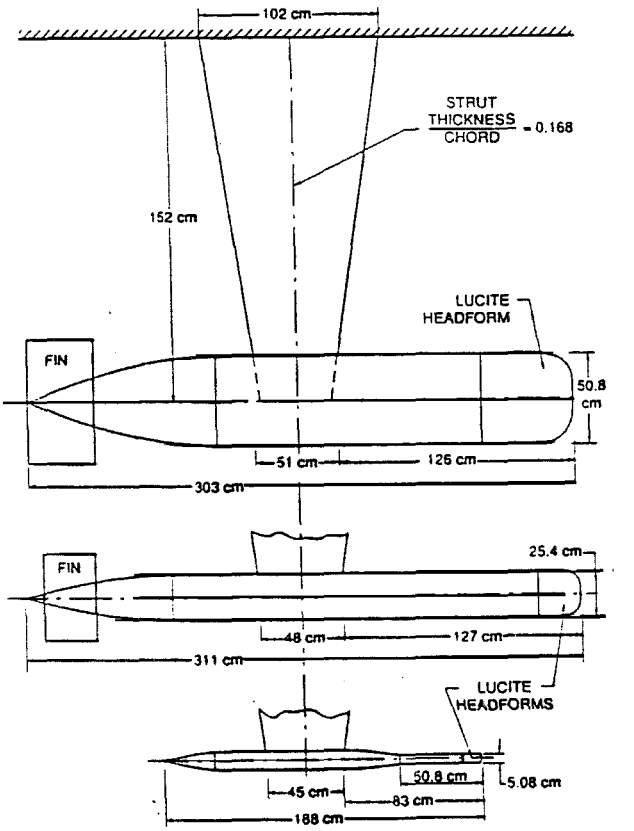

Fig. 3 Schematic diagram the three headforms with afterbodies and supporting strut.

Electrode bubble detection

Silver epoxy electrodes were installed flush in the lucite headform. A pattern of alternating voltages is applied to the electrodes, and the electric current from each is monitored. When a bubble passes over one of the electrodes, the impedance of the flow is altered, causing a drop in current which can be detected (Ceccio 1989). Thirteen of these electrodes take the form of small patches (about 1mm in diameter) at different axial locations. In addition, three ring electrodes covering the entire circumference of the body were installed at a particular axial location in order to measure the cavitation event rate over the entire headform. Each one of the signals from the 16 electrodes were connected to both a peak detector trigger box and a computer data acquisition system.

High speed photography and flash

Two cameras triggered simultaneously were set up in order to take flash pictures of individual cavitation bubbles at different angles and different enlargements. Four powerful EGG SS166 flash heads with SS162-165 energy storage racks were used. The film exposure time was of the flash duration and was measured to be about 30μs. Triggering could be done either manually or through a computer controlled lock-out system in series with the electrode peak detector signal.

In addition, a CCD video camera was focused on the top surface of the headform. The EGG flash heads were used in strobing mode, synchronized with the video camera framing rate in order to make a video recording for each operating condition.

Test conditions

The test matrix included three saturation air contents of 80%, 50% and 30% for each of the three Schiebe headforms. The measurements were taken at three velocities of 9m/s, 11.5m/s and 15m/s, allowing a Reynolds number range from 0.54×10^6 to 9.41×10^6. For each velocity about five cavitation numbers were investigated, ranging from bubble inception to fully attached cavitation.

3. CAVITATION INCEPTION DATA

Cavitation inception was defined as the occurrence of some minimum cavitation event rate over the entire body. The first cavitation pattern that was observed at inception for this type of headform consisted of individual traveling bubbles. The event rate could, therefore, be easily monitored by the means of the electrode system located in the bubble growth region of the body. We arbitrarily defined inception as corresponding to a minimum of one event every 5 seconds detected by the upstream patch electrode. Figure 4 shows the values of the cavitation inception number σ_i for all the velocities, headforms and air content measured.

We note that the cavitation inception number increases with the headform diameter and the air content. Cavitation inception therefore occurs at higher pressures as the number of cavitatable free stream nuclei increases. We can define a cavitatable free stream nuclei as one whose pathline intercepts a low enough pressure region above the headform, causing it to explode. As the diameter of the headform, D, increases, the flow rate trough the low pressure region increases like D^2, causing more nuclei to be excited. The decrease of σ_i with the velocity is somewhat surprising and can be explained in the following way. In order to achieve the same cavitation number for all velocities the pressure relative to the vapor pressure, $P-P_v$, has to be varied with $1/U_\infty^2$. For lower velocities the absolute pressure of the flow needs to be substantially less. Lower pressures force the dissolved gas to come out of solution and thus increase the size and number of free stream nuclei available. At the lowest pressures for the 5.08cm headform, the free stream gas bubbles are of the same order in size as the bubble cavitation on the headform, making it extremely difficult to differentiate one from the other. We observe that when the pressure is sufficiently low for the smallest headform to reach inception, the larger headforms already exhibit quite extensive cavitation patterns. The interesting range of cavitation numbers therefore varies considerably from one headform to another.

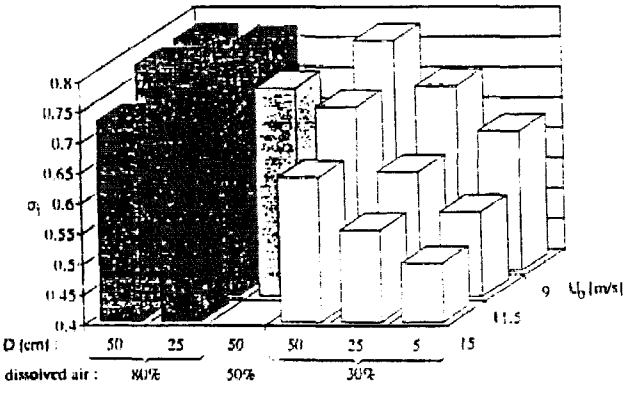

Fig. 4 Cavitation inception numbers σ_i, for the various headform sizes, velocities and air contents.

4. CAVITATION APPEARANCE

A typical bubble cavitation event consists of the growth and collapse of a bubble as it travels through the low pressure region close to the headform surface. The shape and size the bubble will assume is dependent on the cavitation number and the pressure coefficient history it experiences along its trajectory. For each operating condition, individual cavitation bubbles were observed and measured both with high speed photographs and with video recordings. The following observations were made at a dissolved oxygen content of 30%.

Bubble shape

For cavitation numbers close to the minimum pressure coefficient $-Cp_{min}=0.78$, the bubble life-time appears extremely short. In figure 4 we see that the highest inception cavitation numbers σ_i occur for the largest bodies at the lowest velocities. Figure 5a shows a cavitation bubble for such conditions ($\sigma_i=0.77$; D=50.8cm; 9m/s; 30% air content). All the bubbles assume a very thin disk-like geometry. For such cavitation numbers there is little or no growth normal to the headform surface. The bubbles grow almost entirely in the plane parallel to the headform. In its final phase the center of the bubble does not collapse first. Instead we observe the evanescence of the bubble's leading edge. There seems to be a location on the headform at which the cavity collapses, creating a fairly straight leading edge on the bubble. At these cavitation numbers we can see from figure 2, that the critical isobar $Cp=-\sigma$ appears very elongated and close to the body surface. The region below vapor pressure is quite similar to the shape the bubbles assume. It appears that the bubbles are prevented from growing in the direction perpendicular to the body surface by the high normal pressure gradients. The inception cavitation number for the smallest headform is 0.62 at 9m/s and 0.5 at 15m/s and is therefore far from 0.78. For this headform size, even at inception conditions, we do not observe the flat bubble shape of figure 5-a.

As the cavitation number is further decreased, the bubbles grow in volume (in diameter and in height). In some photographs we can observe bubbles in the early growth stage quite distant from the headform and presenting a fairly spherical shape. Rapidly though, their growth appears to interfere with the headform surface, and eventually all the bubbles will adopt a hemispherical cap shape seen in figure 5b. The maximum volume is mostly cavitation number dependent, increasing with lower pressures. As those bubbles approach their collapse phase their thickness, δ, normal to the headform surface decreases faster than their base radius, R, and the leading edge collapses most rapidly along a fairly straight front (figures 5j, 5l). They appear thin and close to the headform surface. This kind of phenomenon has also been observed by Ceccio in previous experiments on the 5.08cm headform. The bubble shape is then quite similar to the one observed at inception conditions for high cavitation numbers.

On most bubbles we observe the presence of wave-like circular dimples at the top of the cap (figures 5b, 5e, 5f, 5g, 5j, 5l, 5m). They seem to become more pronounced as the volume of the bubble increases. The dimples are absent during the growth phase as seen in figure 5c, and appear early in the collapse phase. Their ring shape could be interpreted as a precursor of a collapsing reentrant jet formed early in the collapse phase, but we notice that the center of the dimple retains a concave curvature at all times. The dimple seems quite stable, and remains on the bubble until the very last stage of collapse. For the 50.8cm headform the dimples sometimes appear in pairs on the largest bubbles. On the smallest headform they do not form as distinctly; occasionally we observe a single rough depression in the center of the bubble.

Observations of bubbles on all three headforms shows that their radius at the base of the hemispherical cap, R, scales linearly with the headform diameter, D. At the same cavitation number, the ratio, r=R/D, appears to be the same for all three headforms. We do not observe any variation of r with the velocity U_∞. Furthermore we also notice that the dimensionless collapse location $x_c=X_c/D$ is approximately the same for all headforms. This appears to be true as long as the interactions between bubbles, or between bubbles and patch cavities remains limited. Therefore simple size scaling of the base diameter of the bubble cap with the geometry size seems to be possible. This simple scaling applies only to the bubble's base radius though, since the shape of the bubble, its thickness δ, the amount of shear on its base and the cavitation event rate vary greatly from one headform to the other.

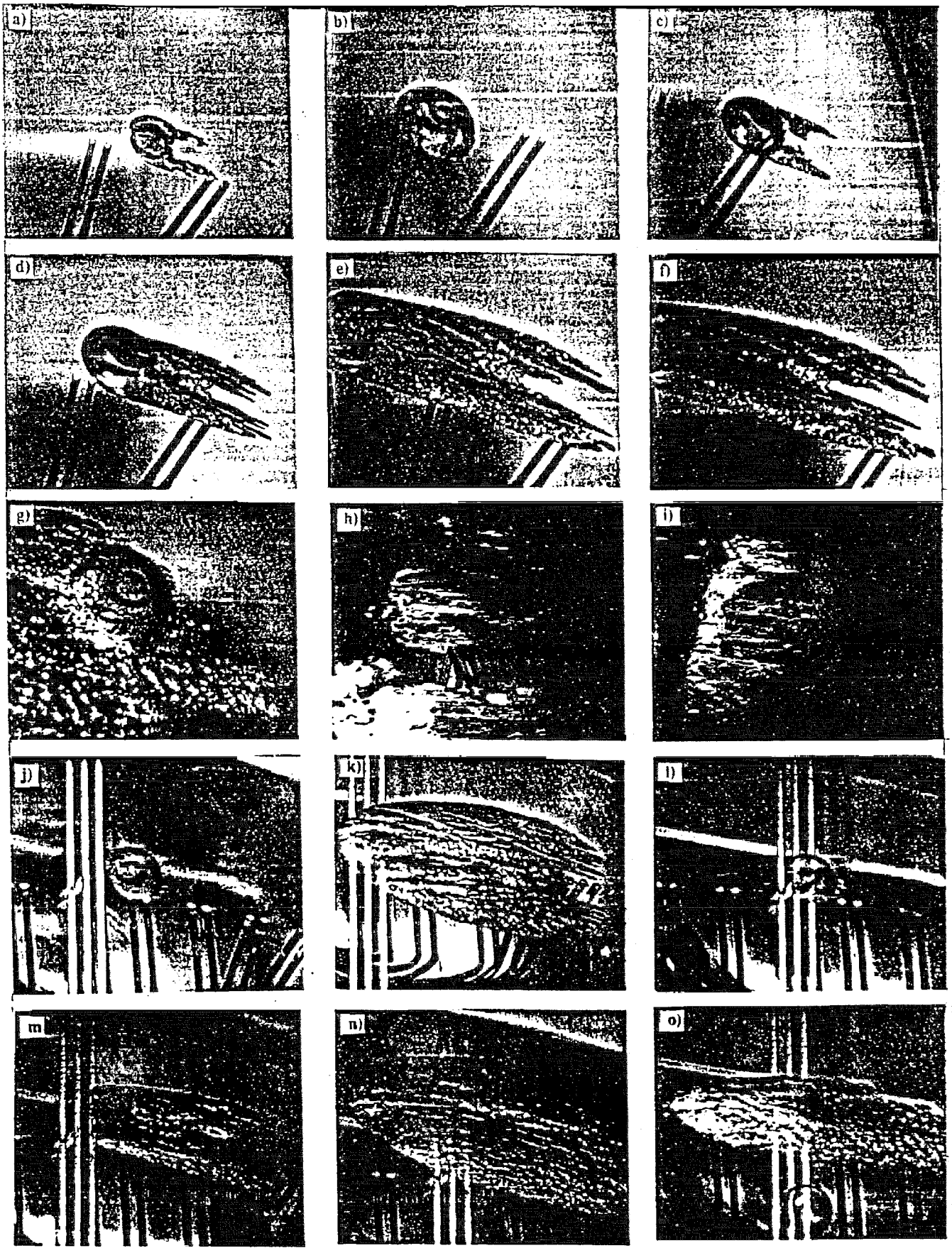

Fig. 5 High speed photography of cavitation events taken at a 30% saturation dissolved air content:
50.8cm diameter headform (distance between the two pairs of patch electrodes: 2.54cm) :
Figure a: U_0=9m/s, σ=0.77; Figures b-c-d-e-f: U_0=15m/s, σ=0.60; Figures g-h: U_0=15m/s, σ=0.54; Figure i: U_0=15m/s, σ=0.51
25.4cm diameter headform (distance between the two pairs of patch electrodes: 1.27cm) :
Figures j-k: U_0=15m/s, σ=0.55; Figures l-m-n: U_0=15m/s, σ=0.53; Figure o: U_0=15m/s, σ=0.49

Bubble tail and patches

Figure 5a shows the presence of streaks of vapor shed behind both sides of the bubble. It appears as though the bubble is sheared in the region extremely close to the headform surface leaving tails behind in its wake. The undersides of some bubbles appear roughened towards the trailing and leading edges. The structure of the tails is always extremely wavy, turbulent, and seems to "stick" to the headform surface (Fig. 5c). The tails may be a result of the breakup of the thin layer separating the bubble from the headform surface. They first appear in the low pressure region, early in the growth phase of the bubble. As the bubble is convected downstream it continues to "feed vapor" into the tails allowing them to extend in length and height (Figures 5c, 5d, 5e, 5f). Ultimately the larger bubbles will collapse leaving behind patch-like cavities. It seems clear that whether a bubble will be sheared or not is determined early in the growth phase. If a bubble does not exhibit the trailing edge streaks early in its passage as seen in figure 5c, it will grow and collapse with a smooth cap shape(Fig 5b, 5j, 5l). Therefore, for fixed cavitation conditions, the streaks always occur around the same position on the headform (Fig. 5c, 5d, 5e, 5f and Fig. 8). For this reason the leading edge of the patches also occur at the same location. If the thickness of those streaks is small, the dynamics of the final collapse of the bubble appears unaffected by them and similar to the process described in the previous paragraph and seen in figure 5m. However, for small enough cavitation numbers the patch can out-grow the bubble and swallow it leaving behind a patch-like cavity (Fig. 5k, 5n). At this point it is not clear if all the patch cavitation structures are generated by traveling bubbles. Some of them evidently are, and can be recognized by a planform shape, similar to a "V" with its vertex pointing downstream. The final length and thickness of the patch cavity is dependent on the bubble that generated it, and therefore varies with the headform diameter and cavitation number. For cavitation numbers close to the minimum pressure coefficient Cp_{min}, no patches and very few bubble tails are observed as in figure 5a. For these conditions the tails seem unable to grow sufficiently to form a patch-like cavity. Figures 5k, 5n show two typical patches at lower cavitation numbers. We notice that the patch on figure 5k is thinner and ends sooner for higher cavitation numbers. The collapse mechanism of the patch itself is quite unclear. In the video recordings they vanish entirely between two frames (1/30 seconds). Is the entire patch swept downstream once the bubble head has vanished, or does it entirely collapse on the headform? The current investigation has not, as of yet, been able to answer these questions.

The number of sheared bubbles seems to increase with the cavitation number, headform diameter and flow velocity. Since the ratio of the laminar boundary layer thickness to headform size will scale with $Re^{-1/2}$, we would expect that the shearing of the cavitation bubbles would increase as the relative boundary layer thickness decreases. However, at the highest Reynolds number of 10^7, we note that the theoretical laminar to turbulent transition comes close to the low pressure region and might cause further disruptive effects.

Bubble-patch interactions

When the cavitation number is sufficiently reduced, the transient patches become fairly stable and remain on the headform, thus creating attached cavities for periods of up to a few seconds. As their number increases the patches will merge to create larger attached structures. Favre and Avellan (1987) have shown that those attached cavities disturb the initial pressure distribution in such a way that they actually extend downstream beyond the original $Cp=-\sigma_i$ isobar. The cavitation number at which this phenomenon happens varies considerably from one headform to the other. It can be seen in figure 5i at a cavitation number of about 0.5 for the 50.8cm headform. By contrast at the same cavitation number the 25.4cm headform produces just a few bubbles and patches (fig. 5o) and the 5.08cm headform shows no cavitation. At this point we note that the transient cavitation patch phenomenon was never observed on the smallest headform. That headform seems to exhibit an abrupt switch from traveling bubble cavitation (some of which have long trailing tails) to persistent attached cavities. The attachment location of these cavities on that headform is fixed, and usually corresponds to a roughness element. This has not been observed on the larger headforms, even though the polished finish was identical to that of the 5.08cm body. Roughness appears to be a very critical parameter for the attached cavitation scaling of these bodies.

For all test conditions at cavitation number below 0.7 we noticed the coexistence of the two different kinds of cavitation patterns: traveling bubbles and transient patches. Quite remarkably, even for the conditions at which we observe many patch-type cavities, some very smooth hemispherical traveling bubbles are still present (fig. 5b, 5h). We can see in figures 5g, 5h, 5i bubble type cavitation riding above attached cavities.

Comparing the shape of the bubbles riding the patch cavities with the others, it is clear that the shapes differ because the former are not subjected to the boundary layer shear which the latter experience. Indeed their exterior shape is close to spherical. These bubbles will eventually collapse and merge completely with the attached cavity upstream of its closure region. By doing so they appear to blow on it and perturb the attached cavity shape as has been observed by Briancon-Marjollet et al. (1990).

5. BUBBLE DIMENSIONS

In order to examine the relative size of the bubbles on the three headforms and at different cavitation numbers various bubble dimensions were measured from the still photographs and the video tape. The base of an individual bubble (surface next to the headform) being close to circular, that dimension was characterized by the radius at the point of maximum bubble growth, R_{max}. The height, δ, of the bubble in a direction normal to the headform surface was also estimated, as was the location of bubble collapse as an axial distance, x_c, from the front stagnation point. First we present in figure 6, the ratio of maximum base radius to headform diameter, $r_{max}=R_{max}/D$. For all three headforms, this non-dimensional bubble size parameter remains roughly the same for a fixed cavitation number. Furthermore, we can see that the velocity has very little influence on the non-dimensional bubble size. This result follows from the Rayleigh-Plesset equation for spherical bubble growth. Once the nuclei has begun to grow, viscous (Reynolds number) and surface tension (Weber number) effects soon become negligible and the dimensionless bubble growth rate, $(dR/dt)/U_0$ (where R is the spherical bubble radius, and U_0 is the reference free stream velocity) depends only on the pressure coefficient history, $Cp(t)$, and the cavitation number, σ. Moreover the time available for growth in the low pressure region scales like D/U_0 and so the equations yield values for R_{max}/D which depend only on the headform shape (as manifest in Cp) and σ. To obtain the necessary input to this calculation, namely Cp along a streamline, the potential flow around the Schiebe headform was obtained using a panel method. Substitution of the pressure coefficient history on a streamline close to the headform surface into the Rayleigh-Plesset equation produced the theoretical result included in figure 6. It is remarkable that, despite the very non-spherical shape of the actual cavitation bubbles, the Rayleigh-Plesset equation yields values which are close to the base radii of the actual bubbles. It is as if the headform surface acts as a plane of symmetry for the growth of the bubble and the pressure gradients parallel to the surface are the sole driving terms.

The only data in figure 6 which departs substantially from the rest is that for the 5.08cm headform at 9m/sec since the gas coming out of solution at this condition makes an accurate reading of the small bubble radius difficult. Finally we note that for inception conditions the bubbles on the smaller headform appear larger relative to the size of the headform because the inception cavitation number σ_i is lower for that smaller headform.

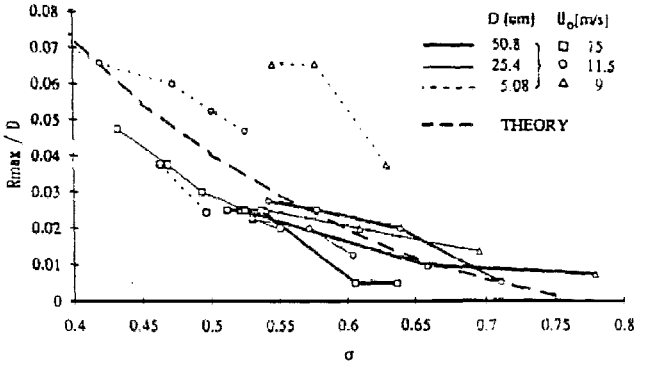

Fig. 6 Bubble maximum radius

The bubble sphericity as measured by $\varepsilon=\delta/R$ at the point of maximum growth of the bubble, also changes substantially with cavitation number as seen in figure 7. The difference in sphericity between the two larger headforms at the same cavitation number is not clear. On the larger diameter headforms, we observed that bubbles appeared extremely thin for cavitation numbers close to inception. The Cp distribution curves above the headform in figure 2, show that the isobars near the minimum pressure region Cp=-0.78 are extremely elongated and close to the surface. Hence there exists a high pressure gradient normal to the surface. Rayleigh-Plesset calculations for a nuclei experiencing pressures along a streamline extremely close to the headform show that for cavitation numbers higher than 0.6, a bubble would grow to a radius that exceeds the height of the critical isobar Cp=-σ. This over-pressure exists over the entire lifetime of the bubble. The three dimensionality of the bubble for those conditions therefore has to be very important. For smaller cavitation numbers, the critical isobar is considerably further from the headform surface and it transpires that even the top of the bubble experiences pressures below the vapor pressure for some time, allowing it to grow in the direction normal to the headform surface. But even in this case the pressure gradient normal to the surface remains much larger than that parallel to the surface (figure 2) and the bubble height δ, in the direction normal to the headform surface, will decay faster than its base radius R in the collapse phase. Therefore the sphericity of a bubble will always decrease towards the collapse phase and this for any cavitating condition.

The cavitation inception number for the 5.08cm headform is around 0.55 . Therefore all the bubbles we have observed on this headform are quite hemispherical since the Cp=-σ isobar is far from the surface at this cavitation number.

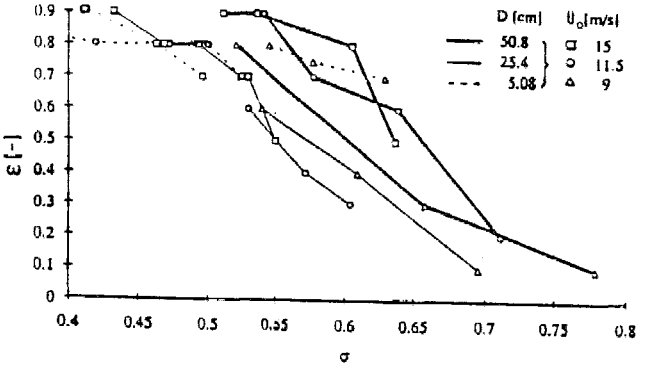

Fig. 7 Bubble sphericity at the maximum growth phase

The influence of the Reynolds number on non-dimensional the attachment location of cavitation $x_a=X_a/D$ is shown in figure 8.

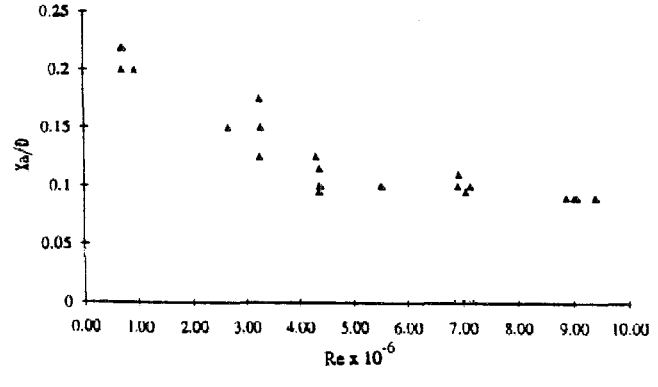

Fig. 8 Attachment point axis coordinate for all headforms and cavitation numbers

The data on that figure includes measurements made on all three headforms and all cavitation numbers. This attachment position appears to be the same for both trailing tails on traveling bubbles, for the leading edge of transient patches or for the separation of attached cavities. We note that this location is mostly Reynolds number dependent, and is very little affected by the cavitation number.

Measurements of the non-dimensional location of bubble collapse as represented by X_C/D, are presented in figure 9 and exhibit a clear dependence on cavitation number with little dependence on the body diameter or the free stream velocity. The Rayleigh-Plesset calculations provided similar results and the location of collapse is in fair agreement with the observations. For cavitation numbers higher than 0.55, the agreement is very good and remains so as long as the bubble does not interact with an attached cavity. As soon as the transient patches or attached cavities appear (σ less than about 0.55), the pressure distribution is modified and the bubbles tend to merge into these cavities at locations further upstream.

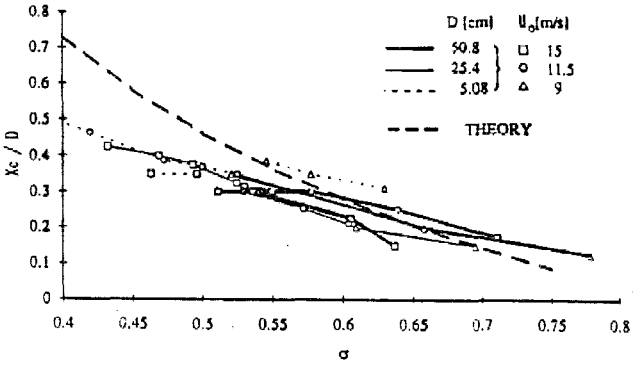

Fig. 9 Bubble collapse location

As the cavitation number is reduced the number of cavitating bubbles appearing on the surface in a still photograph increases. The fraction of the surface in the low pressure region which is covered by bubbles was estimated from the pictures and plotted against σ in figure 10. Note that the increase in the void fraction at lower σ is mostly due to the presence of patches and attached cavities; bubbles do not contribute significantly to this void fraction. Examining this graph, we see that the void fraction increases with headform diameter. Clearly this void fraction is going to depend on the cavitation nuclei number distribution in the incoming stream, and we discuss the consequences of this on the event rate later. However this data was all obtained with similar nuclei populations and so we should address the possible reasons for the trend toward an increasing number of patches or extent of attached cavitation for larger headforms and lower velocities. While the explanation is not at all clear it seems reasonable to suggest that this trend is related to the boundary layer thickness in the region in which cavity attachment may occur. If attachment were related to the ratio of the boundary layer thickness (proportional to $(D/U)^{1/2}$) to the size of a typical roughness (same for all headforms) then this might explain the observed trends.

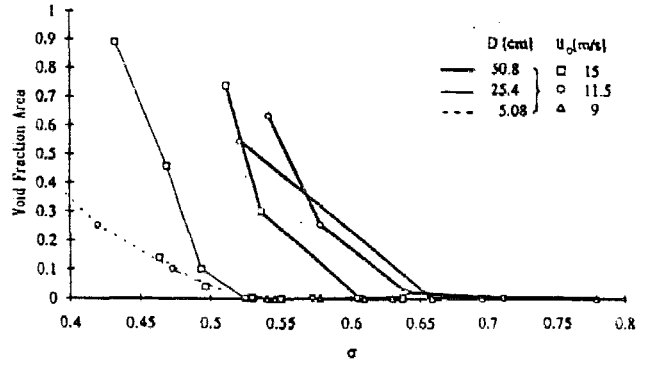

Fig. 10 Average void fraction area over the nose of the headform

6. SOME OBSERVATIONS OF THE CAVITATION EVENT RATE

The photographic and videotape records of the headform cavitation were also analyzed in order to compare the cavitation event rates for the different headform sizes and flow velocities. By counting the number of individual bubbles (or events) observable in a single frame and averaging this number over many frames, we constructed the data of figure 11 in which the average number of events observed on the headform are plotted against cavitation number. Not surprisingly the number of events at a given σ increases with headform size. It also increases with the decrease in speed, an effect which is due to the fact that, at the same cavitation number, a lower speed implies a lower tunnel pressure and therefore more potential nuclei (larger both in number and in size).

It is interesting to evaluate the event rate (or number of events per second) by dividing the ordinates of figure 11 by the bubble lifetime obtained from knowledge of the location of collapse (Figure 9) multiplied by the fluid velocity. If we then divide this data by D^2U_o in order to create a valid comparison for the different sizes and speeds, we obtain the data presented in figure 12 on the number of cavitation events per volume of water.

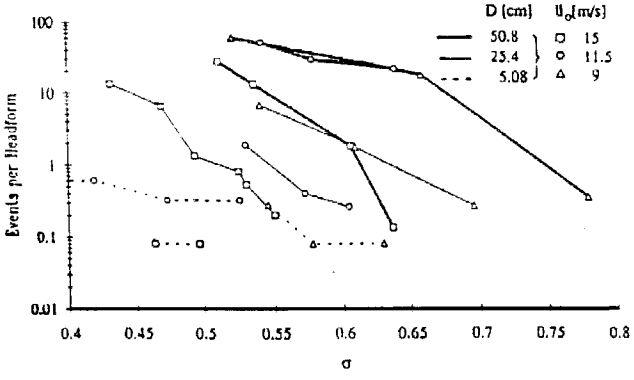

Fig. 11 Average number of events per headform

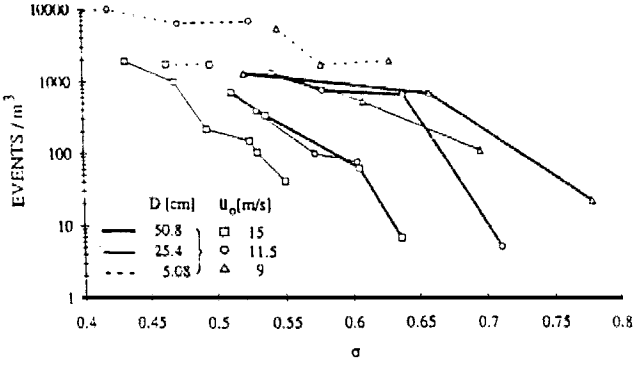

Fig. 12 Cavitation event per volume of water

We observe an increase in cavitation activity as the cavitation number decreases. Two factors may contribute to this increase. As σ decreases smaller nuclei become also subject to cavitation. Also the isobars $Cp=-\sigma$ above the headform extend further in the flow for lower σ values, thus increasing the volume of water passing through the low pressure region. Some other trends are quite surprising in this graph. As the velocity increases the number of free stream nuclei passing through the cavitatable low pressure region should increase linearly and one would therefore expect an increase in the event rate in figure 11 and comparable event per volume in figure 12. We actually observe a substantial decrease in bubble cavitation event rate as the velocity goes from 9 to 11.5 and 15 m/s. This occurs in the data for all three headforms. This trend is consistent with the previously described influence of the velocity on the cavitation inception number. The trends are consistent since the inception number is normally judged in part by the observed event rate. As previously remarked these trends result from the fact that, for a given cavitation number, lower tunnel velocities imply lower tunnel pressures and these in turn lead to an increase in the size and number of cavitation nuclei. During this program, measurements were made of the nuclei number distributions and this data will be correlated with the event rate in later reports.

7. CONCLUSIONS

The cavitation patterns observed on the different sizes of headform appear drastically different. For the same air content, velocity and cavitation number one can observe bubble inception on the smallest headform, and fully attached cavitation on the largest one. The present experiment were designed to reveal differences in the dynamics of traveling bubble cavities as the scale of the flow (or headform) and the velocity of the flow are changed. The Large Cavitation Channel (LCC) of the David Taylor Research Center was used for the observation of cavitation on Schiebe Headforms 5.08, 25.4 and 50.8cm in diameter.

The cavitation inception numbers, σ_i, for these headforms were all less than $-Cp_{min}$ and, for different speeds and sizes, showed a clear and coherent dependence on Reynolds number, Re, with σ_i decreasing as Re increased. The differences in appearance of the cavitation on the three headforms, could be attributed in part to the differences in σ_i. However it was also clear that the complex flows around individual traveling bubbles and their interaction with the boundary layer are influenced by Reynolds number (and Weber number) effects. Virtually all the traveling bubbles on all the headforms were of the spherical cap shape described earlier by Ceccio and Brennen (1991). Many of the detailed phenomena described in that paper were also present on the larger headforms. Among these phenomena were the shearing of the surface of the bubble next to the surface, the fissioning of bubbles during collapse and the eventual emergence of one or more small transverse vortices with vapor filled cores. Also observed was the phenomenon of bubble induced attached cavities or "tails". On the smaller headform (lower Re) these tended to occur at the lateral extremes of the bubble producing two trailing (or wing-tip) cavities attached to the surface near the cavity attachment point and being stretched out behind the bubble. On the larger headforms (larger Re) they tended to rapidly degenerate and extend over the entire width of the passing bubble. At low cavitation numbers, σ, we observed "patches" of attached cavities rather than the more limited "tails". The patch tended to be very ephemeral at higher cavitation numbers. At lower σ it persisted longer and, at low enough σ remained indefinitely attached. This provides one explanation for the origin of patch cavitation though it may not be the only one. Another new observation during the present experiments was the appearance of a remarkably repeatable "dimple" on the exterior surface of the traveling bubbles on the two larger headforms. These seem to appear when the actual bubble becomes sufficiently large which suggests that they are influenced by surface tension.

The present paper has presented detailed data on the dimensions of these traveling bubbles and shown that, despite the radical departures from spherical symmetry, the overall dimensions and the location of separation are surprisingly close to those predicted by the Rayleigh-Plesset equation. In section 6 we have presented some preliminary data on the event rates and how they scaled with headform size, velocity and cavitation number. Later papers will focus on the relationship between the cavitation event rates and the cavitation nuclei population in the channel during these experiments.

ACKNOWLEDGMENTS

Large scale experiments like these require help of many people and the authors are very grateful to all of those who helped in this enterprise. We are very grateful to the ONR for their support under contracts N00014-91-J-1426 (SLC) and N00014-91-J-1295 (CEB, YKdC). We are also extremely grateful to the David Taylor Research Center (DTRC) and to their staff including W. B. Morgan for making the use of the LCC possible for us. From DTRC both Scott Gowing and James Blanton were important and valued members of the team who conducted the experiments. Po-Wen Yu (U. of Michigan) and Douglas Hart (Caltech) provided important help with the experiments. The staff at the LCC in Memphis, Tenn. were remarkably tolerant and invariably helpful and we wish to thank all of them most sincerely; we are particularly grateful to Bob Etter whose constant support was invaluable.

REFERENCES

Arakeri, V.H. and Shanmuganathan, V. 1985. *On the evidence for the effect of bubble interference on cavitation noise.* J. Fluid Mech., Vol. 159, pp. 131-150.

Brennen, C.E. and Ceccio, S.L. 1989. *Recent Observations on cavitation and cavitation noise.* Proc. ASME Third Int. Symp. on Cavitation Noise and Erosion in Fluid Systems, San Francisco, FED-Vol. 88, pp. 67-78.

Briancon-Marjollet, L. and Franc, J.M. 1990. *Transient bubbles interacting with an attached cavity and the bounaary layer.* J. Fluid Mech., Vol. 218, pp. 355-376.

Blake, W.K., Wolpert, M.J. and Geib, F.E. 1977. *Cavitation noise and inception as influenced by boundary layer development on a hydrofoil.* J. Fluid Mech., Vol. 80, pp. 617-640.

Ceccio, S.L. 1989. *Observations of the dynamics and acoustics of traveling bubble cavitation.* Ph.D. Thesis, California Institute of Technology.

Ceccio, S.L. and Brennen, C.E. 1991. *The dynamics and acoustics of traveling bubble cavitation.* J. Fluid Mech., Vol. 233, pp. 633-660.

D'Agostino, L., Brennen, C.E. and Acosta, A.J. 1988. *Linearized dynamics of two-dimensional bubbly and cavitating flows over slender surfaces.* J. Fluid Mech., Vol. 192, pp. 485-509.

Favre, J.N., Avellan, F., Ryhming, I.L. 1987. *Cavitation performance improvement using a 2-D inverse method of hydraulic runner design.* Proc. Int. Conf. on Inverse Design Concepts and Optimization in Engineering Science-II., Penn. State Univ.

Kumar, S. and Brennen, C.E. 1991. *Statistics of noise generated by traveling bubble cavitation.* ASME Cavitation and Multiphase Flow Forum, Portland OR, June 1991. FED Vol. 109, pp. 55-62.

Kumar, S. and Brennen, C.E. 1992. *An acoustical study of traveling bubble cavitation.* Submitted to J. of Fluid Mech.

Lindgren, H. and Johnsson, C.A. 1966. *Cavitation inception on headforms. ITTC comparative experiments.* 11th Int. Towing Tank Conf., pp. 219-232.

Meyer, R.S., Billet, M.L. and Holl, J.W. 1989. *Free-stream nuclei and cavitation.* Proc. ASME Third Int. Symp. on Cavitation Noise and Erosion in Fluid Systems, San Francisco, FED-Vol. 88, pp. 52-62.

Morgan, W.B. 1990. *David Taylor Research Center's Large Cavitation Channel.* Proc. Int. Towing Tank Conference, Madrid, Spain, pp. 1-9.

O'Hern, T., d'Agostino, L. and Acosta, A.J. 1988. *Comparison of holographic and counter measurements of cavitation nuclei in the ocean.* ASME J. Fluids Eng., Vol. 110, pp. 200-207.

O'Hern, T., Katz, J. and Acosta, A.J. 1985. *Holographic measurements of cavitation nuclei in the sea.* ASME Cavitation and Multiphase Flow Forum Booklet, FED Vol. 23, pp 39-42.

Schiebe, F.R. 1972. *Measurements of the cavitation susceptibility of water using standard bodies.* St. Anthony Falls Hydraulic Lab., Univ. of Minnesota, Rep. No. 118.

Vogel, A., Lauterborn, W. and Timm, R. 1989. Optical and acoustic investigations of dynamics of the Laser-produced cavitation bubbles near a solid boundary layer. J. Fluid Mech., Vol. 206, pp. 299-338.